Since January 2020 Elsevier has created a COVID-19 resource centre with free information in English and Mandarin on the novel coronavirus COVID-19. The COVID-19 resource centre is hosted on Elsevier Connect, the company's public news and information website.

ELSEVIER

Bone 39 (2006) 863–871

BONE

www.elsevier.com/locate/bone

Multiple bioimaging modalities in evaluation of an experimental osteonecrosis induced by a combination of lipopolysaccharide and methylprednisolone

L. Qin [a,*], G. Zhang [a], H. Sheng [a], K.W. Yeung [b], H.Y. Yeung [a], C.W. Chan [a], W.H. Cheung [a], J. Griffith [b], K.H. Chiu [a], K.S. Leung [a]

[a] *Musculoskeletal Research Laboratory, Department of Orthopaedics and Traumatology, The Chinese University of Hong Kong, Hong Kong SAR, PR China*
[b] *Department of Diagnostic Radiology and Organ Imaging, The Chinese University of Hong Kong, Hong Kong SAR, PR China*

Received 27 January 2006; revised 31 March 2006; accepted 7 April 2006
Available online 12 June 2006

Abstract

Aims: The present study employed both static and dynamic imaging modalities to study both intra- and extravascular events attributing to steroid-associated osteonecrosis (ON) using an experimental protocol with a single low-dose lipopolysaccharide (LPS) injection and subsequently three injections of high-dose methylprednisolone (MPS).
Methods: Fourteen 28-week-old male New Zealand white rabbits received one intravenous injection of LPS (10 μg/kg). 24 h later, three injections of 20 mg/kg of MPS were given intramuscularly at a time interval of 24 h. Additional 6 rabbits were used as controls. Dynamic MRI was performed on bilateral femora for local intraosseous perfusion before and after LPS injection. Blood samples were collected for hematological examinations before and after LPS injection. Bilateral femora were dissected and decalcified for microCT-based microangiography. ON lesion, intravascular thrombus and extravascular marrow fat cell size were examined histopathologically.
Results: Intravascular thrombus was observed in all ON rabbits. Extravascular marrow fat cell size was significantly increased in ON rabbits than that of the controls ($P<0.05$). Compared to baseline, a significant decrease in ratio of tissue-type plasminogen activator/plasminogen activator inhibitor 1, activated partial thromboplatin time and a significant increase in ratio of low-density lipoprotein/high-density lipoprotein were only found in ON rabbits ($P<0.05$). Dynamic MRI showed a significant decrease in the perfusion index 'maximum enhancement' in the ON rabbits ($P<0.05$), and microCT-based microangiography showed blocked stem vessels in ON samples. Overall, 93% of the rabbits (13/14) developed ON, and no rabbits died throughout the experiment period.
Conclusion: Both intra- and extravascular events were found attributing to the steroid-associated ON based on our experimental protocol with a single low-dose LPS injection and subsequent three injections of high-dose MPS. Both high ON incidence and no mortality in rabbits treated with this inductive protocol suggested its effectiveness for future studies on evaluation of therapeutic efficacy of interventions developed for prevention of steroid-associated ON.

Keywords: Steroid-associated osteonecrosis; Intravascular thrombus occlusion; Extravascular marrow lipid deposition; Perfusion; Ischemia

Introduction

Up to now, pulsed steroids are frequently prescribed as life-saving agent for serious infectious diseases such as Severe Acute Respiratory Syndrome (SARS) and Acquired Immure Deficiency Syndrome (AIDS) [1,2]. Inevitably, it has been reported that steroid-associated osteonecrosis (ON) occurs in those recovered patients from SARS-CoV infection and stabilized patients with AIDS-HIV infection [3,4].

ON refers to death of bone due to ischemia. The pathogenesis of steroid-associated ON might relate to intravascular thrombus occlusion and extravascular marrow lipid deposition, leading to an impaired structure–function of intraosseous blood supply system. In turn, the impaired intraosseous blood supply system might serve the pathophysiologic pathway and induced local

* Corresponding author. Fax: +852 26324618.
E-mail address: Lingqin@cuhk.edu.hk (L. Qin).

8756-3282/$ - see front matter © 2006 Elsevier Inc. All rights reserved.
doi:10.1016/j.bone.2006.04.018

ischemia, necrotic lesion and eventually subchondral bone collapse [5,6]. As surgical prognosis is always problematic for prevention of subchondral bone collapse [7], it is highly desirable to develop intervention strategies for steroid-associated ON. It is therefore highly desirable to establish an appropriate animal model and valid evaluation methods not only related to the 'end-point', i.e. the pathological ON and more importantly the methods for dynamic monitoring of the ON development in studying potential underlying pathophysiologic mechanisms.

There were two classical inductive protocols commonly used for establishing ON rabbits relevant to steroid. One was to use a single injection of high-dose methylprednisolone (MPS) (H-MPS × 1), which showed however rather low incidence of ON (43%) [8]. The other was to use two injections of high-dose lipopolysaccharide (LPS) combined with subsequent three injections of high-dose MPS (H-LPS × 2 + H-MPS × 3), which induced higher ON incidence (85%) but accompanied with high mortality of experimental animals (50%) [9]. In testing intervention strategies for steroid-associated ON, there is a need to develop inductive protocols for establishing ON lesions with a high ON incidence yet low or even no mortality.

Recently, a steroid-independent ON model was successfully established with a single injection of low-dose LPS (L-LPS × 1). This model showed a higher incidence of ON lesion (77%) and lower mortality (11%) in rabbits as compared with the previously published protocol (H-LPS × 2 + H-MPS × 3) due to the avoidance of severe LPS-induced shock by lowering the given LPS dose [10]. Furthermore, the steroid-independent inductive protocol (L-LPS × 1) served as basis for modifying the steroid-associated inductive protocol (H-LPS × 2 + H-MPS × 3). Accordingly, we hypothesized that a single injection of low-dose LPS combined with subsequent three injections of high-dose MPS (L-LPS × 1 + H-MPS × 3) might induce a high incidence of ON but low or even no mortality in rabbits.

For confirming the effectiveness of above purposed inductive protocol for establishment of a steroid-associated ON animal model, the present study was designed to use both conventional and advanced static and dynamic bioimaging methods to investigate the pathogenic events, pathophysiologic pathways and end-points related to ON incidence and mortality in a rabbit model. For pathogenic events, intravascular thrombus and extravascular marrow fat cell size were examined histologically, and coagulation-fibrinolysis and lipid transport were assayed hematologically. For studying pathophysiologic pathways, both function and structure of intraosseous blood supply system were examined by dynamic MRI and microCT-based microangiography. ON incidence and animal mortality were examined by bone histopathology and experimental documentation, respectively.

Materials and methods

Animals, grouping, and treatment

Twenty 28-week-old male New-Zealand white rabbits with body weight of 4–5 kg were housed at the Experimental Animal Center of the investigators' hospital and received a standard laboratory diet and water ad libitum. The experimental protocol was approved by the Animal Experiment Ethics Committee of the Chinese University of Hong Kong (Ref No. 04/038/MIS). Fourteen rabbits assigned into the treatment group were intravenously injected with 10 μg/kg body weight of LPS (*Escherichia coli* 0111:B4, Sigma-Aldrich, Inc. USA). Twenty four hours later, three injections of 20 mg/kg body weight of MPS (Pharmacia and Upjohn, USA) were given intramuscularly at a time interval of 24 h. Six rabbits were used for control group and injected with 0.9% normal saline. It was reported that ON gradually developed and repair process of the necrotic bone also observed 6 weeks after injection of MPS [8], which was similar to stage II of ON clinically (Ficart and Arlet classification system) [11]. The rabbits in both groups were euthanized 6 weeks after the last MPS injection. Mortality of rabbits if any was documented throughout the entire experimental period.

Pre-euthanasia evaluation

Hematological examination

Five milliliters of blood sample was collected in a fasting state from each rabbit through the auricular arteries immediately before injection of LPS, and before the first MPS injection and at 24 h after the last MPS injection. Plasma was obtained by transferring the blood sample into a tube containing 0.5 ml of 3.8% sodium citrate anticoagulant for centrifugation at 3000 rpm for 10 min at 4°C. Half of the plasma was then stored at −70°C for evaluating pre-thrombotic status, including t-PA/PAI-I (ratio of tissue type plasminogen activator to plasminogen activator inhibitor) by enzyme-linked immunosorbent assay technique using corresponding mouse monoclonal anti-human antibodies (Manufacturer's Datasheet, XITANG Biotechnology, Shanghai, China) and APTT (activated partial thromboplatin time) by an automatic blood coagulation analysis device (SysmexCA-50, Japan). The other half was stored at −70°C for evaluating lipid transportation, including LDL/HDL (ratio of low-density lipoprotein cholesterol to high-density lipoprotein cholesterol) [12,13].

Dynamic MRI

Dynamic MRI was performed for bilateral proximal and distal femora before LPS injection and 6 weeks after the last injection of MPS, using a 1.5 T superconducting system (ACS-NT Intera; Philips, the Netherlands). Under sedation with Katamin (0.25 ml/kg, i.m.), the rabbits were placed in supine with the lower limb flexed and fixed by adhesive tape. An extremity coil (transmit–receive surface coil) was used on the target site. Preliminary sagittal and oblique axial images were obtained to define the femoral longitudinal axis. T1-weighted MRI images (T1W, repetition time [TR]/echo time [TE] = 425/13 ms) were used for analysis of the target side. Imaging parameters were as follows: a section thickness of 3 mm, intersection gap of 1 mm, field of view of 120 mm and imaging matrix of 256 × 128. A receive-only surface coil was used to cover the target site during MRI acquisition. The contrast-enhanced dynamic MRI pulse sequence used ultrafast T1-weighted gradient-echo sequences (turbo-field echo; Philips) with TR = 2.2 ms, TE = 0.92 ms, pre-pulse inversion time = 400 ms, flip angle = 15°, scan percentage = 40% and acquisition matrix = 128 × 128. A total of 200 dynamic images were obtained in 90 s. A bolus of dimeglumin gadopentetate (Magnevist; Schering, Berlin, Germany) (0.8 mmol/kg/body

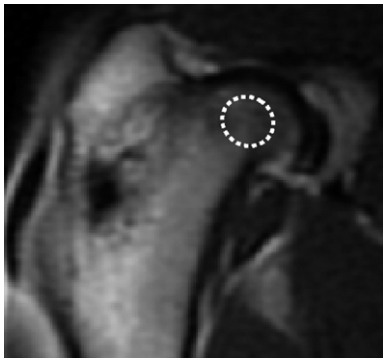

Fig. 1. A T1-weighted coronal MRI image of rabbit proximal femur (TR/TE = 425/13) after Gd-DTPA administration. The region of interest (ROI) in the central part of femoral head with a size of 8–10 pixels (64–80 mm^2) was defined for analysis of local intraosseous perfusion.

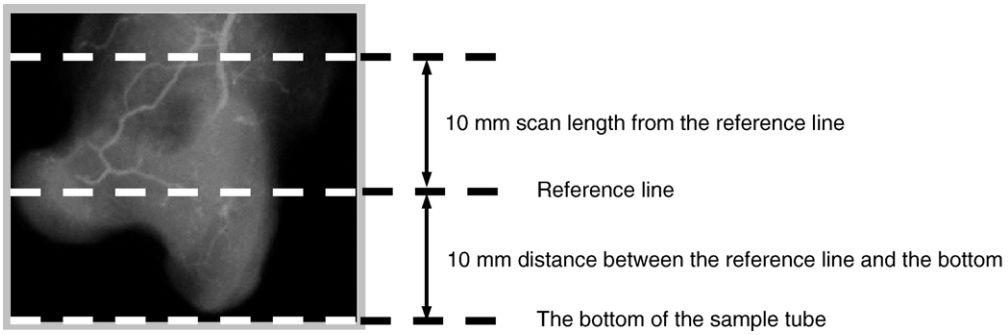

Fig. 2. Positioning of rabbit proximal femur for microCT scanning (radiograph used for illustration) and region of interest (ROI) defined for studying local vasculature.

weight) was rapidly administered manually via a previously placed 21-gauge intravenous catheter in the right ear vein, immediately followed by a 6 ml saline flush at the same injection rate. The dynamic scan started as soon as the injection of the contrast medium commenced. Signal intensity (SI) was then measured in operator-defined ellipse-like regions of interest (ROIs) over the target site beneath the joint space in the mid-coronal T1-weighted images using a cursor and graphic display device (Fig. 1). The SI values derived from the ROIs were plotted against time as time–intensity curve (TIC) using the built-in Gyroview software system. The baseline value (SI_{base}) of the SI in a TIC was calculated as the mean SI value in the first three images. The maximum SI (SI_{max}) was defined as the peak enhancement value at a given time interval of 90 s after contrast injection during the early phase of the first pass. Perfusion index 'maximum enhancement' was calculated as [14]:

$$\text{Maximum enhancement} = \frac{SI_{max} - SI_{base}}{SI_{base}} \times 100\%$$

The mean of the 'maximum enhancement' values measured at bilateral proximal femur or distal femur was used as the one of each rabbit.

Posteuthanasia evaluations

Perfusion and decalcification

Under general anesthesia with 2.5% sodium pentobarbital (0.4 ml/kg), the abdomen cavity of the animals was opened, and a scurf needle with 25 mm syringe was inserted in the abdominal aorta distal to the heart with ligation of that proximal to the heart. The vasculature was flushed with 50 U/ml heparinized normal saline at 37°C and at a flow speed of 20 mm/min via an automatic pump apparatus (PHD 22/2000, Harvard Apparatus, USA) linked to the syringe [15]. As soon as the outflow from an incision of the abdominal vein was limpidness, 10% neutral buffered formalin (37°C) was pumped into the vasculature to fix the nourished skeletal specimen [16]. The formalin was then flushed from the vasculature using the heparinized normal saline, and the vasculature was injected with Microfil, a lead chromate-containing confected radiopaque silicone rubber compound based on the manufacturer's protocol (Microfil MV-122, Flow Tech; Carver, MA, USA). Animals were then euthanized with an overdose of sodium pentobarbital and stored at 4°C for 1 h to ensure polymerization of the contrast agent before microangiography. Bilateral femoral samples were then harvested and fixed in paraformaldehyde (4%) for decalcified with ethylenediaminetetraacetic acid (EDTA, 10%, pH 7.4). Success of decalcification was confirmed by anteroposterior view radiographs taken using a cabinet X-ray system (Specimen Radiography System, Faxitron 43855C, Fraxitron X-ray Corporation, Wheeling, IL, USA) under an exposure condition of 40 kV/30 s. Then, both proximal 1/3 and distal 1/3 of bilateral femoral samples, i.e. four dissected parts for each rabbit, were obtained for evaluations.

Microangiography

With the help of one experienced microCT application specialist, both proximal and distal part of the bilateral femoral samples of each rabbit were placed with proximal and distal end into a polymethylmethacrylat (PMMA) sample tube, respectively. The femoral shaft was fixed in the tube with its long axis perpendicular to the bottom of the tube for microCT scanning using μCT-40 (Scanco Medical, Bassersdorf, Switzerland). The scan was then perpendicular to the shaft and initiated from a reference line 10 mm away from the bottom with an entire scan length of 10 mm (Fig. 2). The scan was preformed at a resolution of 36 μm per voxel with 1024×1024 pixel image matrix. For segmentation of blood vessels from background, noise was removed using a low pass Gaussian filter (Sigma=1.2, Support=2) and blood vessels were then defined at a threshold of 85. In order to reconstruct the three-dimensional (3-D) architecture of vasculature in either the proximal femur or the distal femur, the blood vessels filled with Microfil were included with semi-automatically drawn contour at each two-dimensional (2-D) section by built-in "Contouring Program" for automatic reconstruction of 3-D image of vasculature in the decalcified sample. A histogram was subsequently generated to display the distribution of vessel size, and a color-coded scale was mapped to the surface of the 3-D images to produce a visual representation of the vessel size distribution [16].

Histopathology

After microangiography, all the decalcified samples were embedded in paraffin, cut into 6-μm-thick sections along the coronal plane for the proximal parts and the axial plane for the distal parts. Sections were stained with hematoxylin–eosin (H&E) for evaluation of osteonecrosis and calculation of fat cell size.

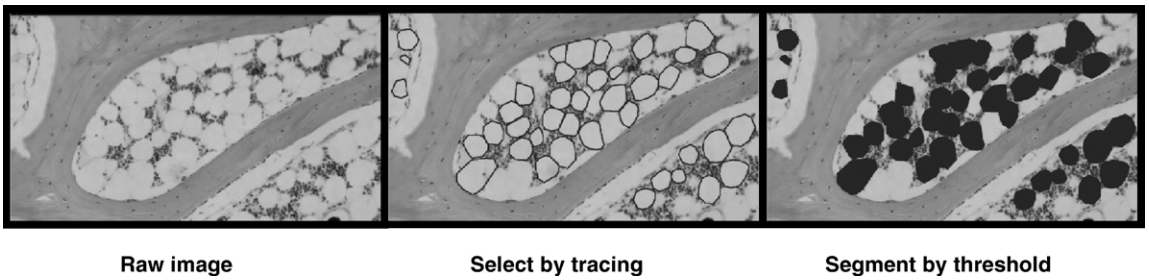

Fig. 3. Imaging process for histomorphometry of bone marrow fat cell size. (A) Visualization of bone marrow after digitalizing a histological section of proximal femur. (B) Marrow fat cells are manually traced using image analysis system. (C) Labeling of the traced marrow fat cells for calculating its Feret's diameter, i.e. the greatest distance between any two points along the boundary of a region of interest.

Phosphotungstic acid hematoxylin (PTAH) was the staining specifically employed for examination of fibrin thrombus [17]. (1) Evaluation of ON: entire areas of each dissected part of bilateral femoral samples, including epiphysis and metaphysis, were examined for the presence of ON, which were judged blindly by two pathologists basis on the characteristic histopathological features with diffuse presence of empty lacunae or pyknotic nuclei of osteocytes in the trabeculae, accompanied by surrounding necrotic bone marrow [8,9]. All rabbits that had at least one osteonecrotic lesion in the examined sections were defined as ON^+, while those with no osteonecrotic lesions were ON^-. (2) Calculation of extravascular marrow fat cell size: the fat cell size of each rabbit was calculated as the average of the Feret's diameter of all bone marrow fat cells with clearly defined profile in 4 randomly selected fields (up–down–left–right) of each dissected part of bilateral femur samples (16 fields for 4 dissected parts from each rabbit). The histological sections were digitized into a microscope imaging system (Zeiss Aixoplan with Spot RT digital camera, Zeiss, Germany) for quantification using image analysis software (ImageJ 1.32j, NIH, USA). Briefly, the fat cells were manually traced and labeled calculating the cell size interpreted by Feret's diameter (Fig. 3), which was the greatest distance between any two points along the boundary of a region of interest [18]. Fat cells that had undergone necrosis were excluded from imaging analysis [10]. (3) Examination of intravascular thrombus: the entire area of each dissected part of bilateral femoral samples was examined for identifying the presence of intravascular thrombus in a blind fashion by two pathologists based on diffuse presence of thrombus stained with PTAH within the marrow vessels. All rabbits that had intravascular thrombus were regarded $PTAH^+$, while those with no intravascular thrombus were $PTAH^-$.

Statistics

The incidence of ON was defined as the number of ON^+ rabbits divided by total number of rabbits in each group. The fat cell size of each group was expressed as mean±SD, and comparison between ON^+ rabbits and control rabbits was performed using Student's *t* test. The follow-up data on both

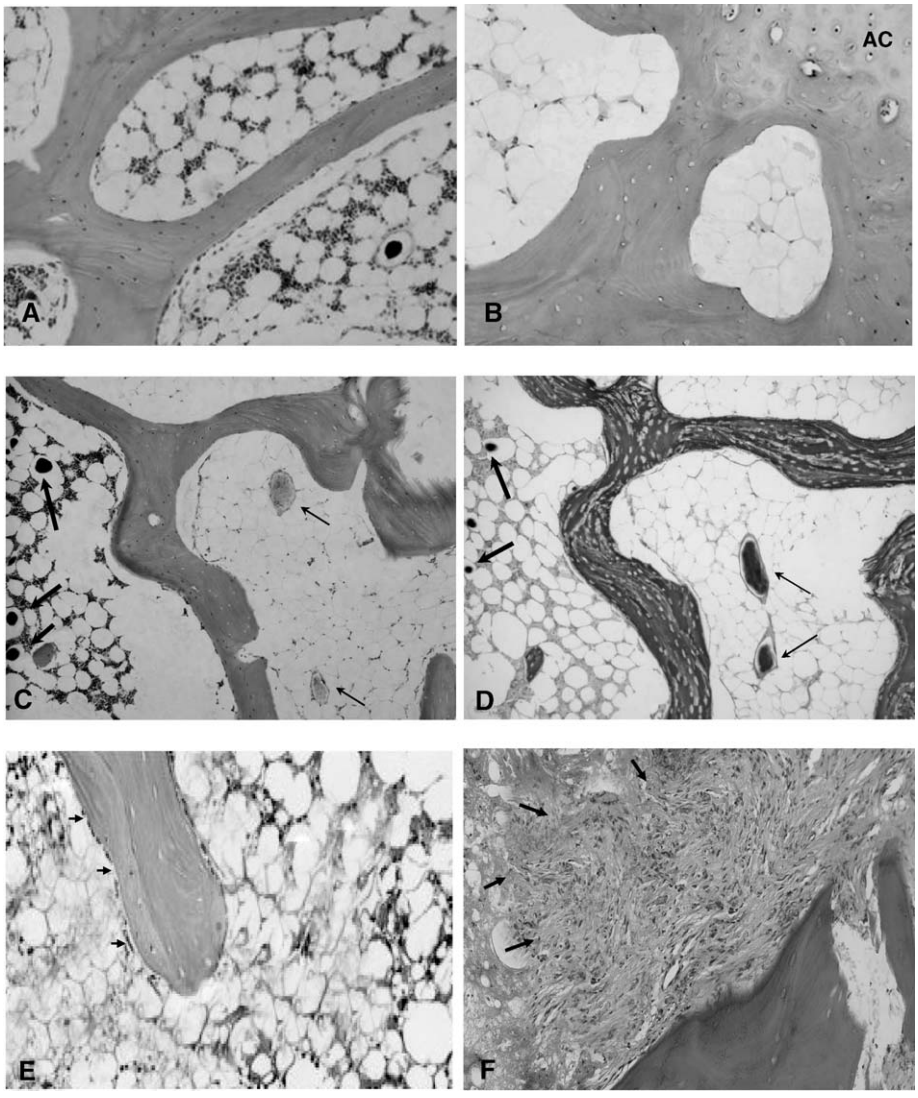

Fig. 4. Histological features of both normal and necrotic bone. (A) Normal bone tissue with intact structural and cellar events (hematoxylin and eosin, ×40). (B) ON lesion at epiphysis: lamellar trabeculae with numerous typical empty lacunae, which are surrounded by large-adipocyte-rich marrow containing amorphism substance (AC: articular cartilage) (hematoxylin and eosin, ×40). (C) Intravascular thrombosis in ON bone: the necrotic lamellar trabecular bone with empty lacunae found next to the ischemic bone marrow, which contains intravascular thrombi (right half, pointed with thin arrows), while the region with relative intact bone marrow (left half) contains intravascular perfusion substance (Microfil) located in sinusoid (pointed with thick arrows) (hematoxylin and eosin, ×20). (D) Ischemic marrow with intravascular thrombi stained specifically with PTAH for intravascular thrombi (right half pointed with thin arrow) and the region with relative intact bone marrow (left half) contains intravascular perfusion substance (Microfil) located in sinusoid (pointed with thick arrows) (PTAH, ×20). (E) Limited repair: appositional bone formation with lining cells (osteoblasts) (indicated with arrow) around the necrotic bone (hematoxylin and eosin, ×40). (F) Destructive repair: granulation tissue creep (pointed by arrow) linked to necrotic bone resorption (hematoxylin and eosin, ×40).

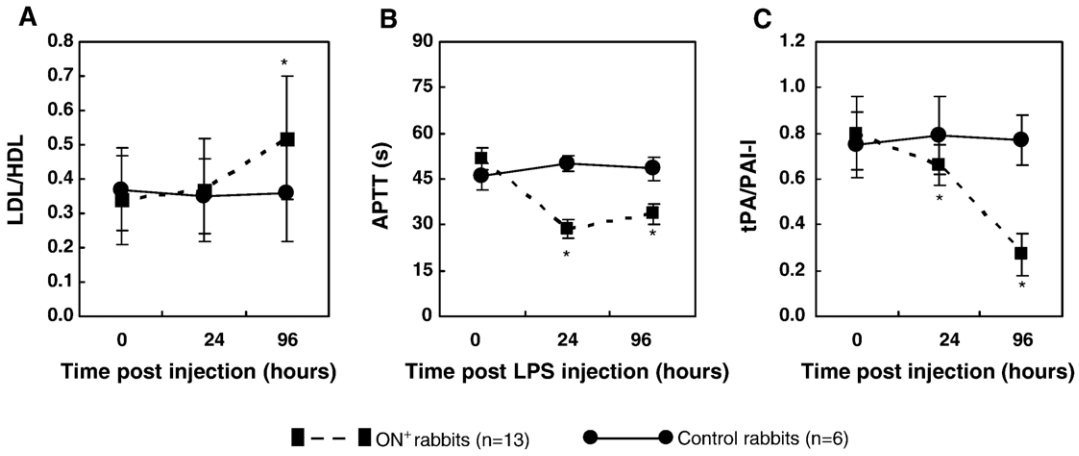

Fig. 5. Time-course changes in the ratio of plasma LDL/HDL (A), APTT (B) and the ratio of plasma t-PA/PAI-I (C) using repeated ANOVA test. *$P<0.05$, compared with 0 h, control rabbits and 24 h, respectively (data in mean and SD). 0 h: immediately before LPS injection; 24 h: 24 h after LPS injection and immediately before the first MPS injection; 96 h: 24 h after the last MPS injection or 96 h after LPS injection.

hematological indicators and dynamic MRI perfusion parameter from each group were analyzed using GLM (General Linear Model)-based repeated measure multivariate analysis of variance (MANOVA). Statistical significance was set at $P<0.05$. All statistical analysis was performed using SPSS 10.0 (SPSS Inc., Chicago, IL, USA).

Results

End-point evaluations

Mortality and ON incidence

Rabbits treated with LPS–MPS were generally found physically less active as compared with control rabbits. No rabbits died of the inductive protocol throughout the experiment period. 93% of the rabbits (13/14) in the treatment group developed ON 6 weeks after last injection of MPS, while no ON lesion was found in control rabbits. In a location-specific histopathological examination for the proximal femora, 86% (24/28) were found having developed ON in the metaphysis while 29% (8/28) developed ON in the proximal epiphysis. As for the distal femora, 93% (26/28) developed ON in the metaphysis and 36% (10/28) developed ON in the epiphysis. ON lesions with typical features were found at either metaphysis or epiphysis in ON^+ rabbits. Destructive repair characterized with either limited repair with appositional bone formation around necrotic bone or granulation tissue creep linked to the resorbing necrotic bone was observed in several ON^+ samples. No subchondral bone collapse was found in all bone samples of ON^+ rabbits. There were no histopathological findings observed in all the control bone samples (Figs. 4A–F).

Intravascular/extravascular pathogenic events

Histopathological findings

(1) Intravascular thrombotic occlusion: thrombi stained with PTAH were only found in small marrow vessels around necrotic bone in all ON^+ rabbits (Fig. 4D). There was no thrombosis found in either the ON^- rabbit or control rabbits. (2) Increased extravascular marrow fat cell size: the Feret's diameter of fat cell in ON^+ rabbits (65.71 ± 6.31 μm) was significantly larger ($P<0.05$) than that of the control rabbits (42.17 ± 2.54 μm) and one ON^- rabbit (46.43 μm). In the control rabbits, considerable space was preserved for marrow hematopoietic cells and vessels, while obvious less space was available for marrow elements due to the enlarged fat cell size in the ON^+ rabbits (Figs. 4B and D).

Hematological findings

In ON^+ rabbits, a significant decrease in the ratio of t-PA/PAI-I before the first MPS injection was found from baseline ($P<0.05$) as a result of LPS induction. Twenty four hours after the last MPS injection, the decreasing tendency of APTT maintained, whereas a rapid decreasing tendency of the ratio of t-PA/PAI-I presented. The ratio of LDL/HDL did not increase significantly from baseline until 24 h after the last MPS injection. No detectable changes ($P>0.05$) were found in the hematological examinations for the control rabbits during the entire study period. There was a significant difference in both the ratio of t-PA/PAI-I and the ratio of LDL/HDL between the ON^+ rabbits and the control rabbits ($P<0.05$) (Figs. 5A–C). Only moderate changes in the above-mentioned hematological examination were presented in one ON^- rabbit, the only one in the treatment group (1/14) in this study.

Pathophysiologic pathway for intraosseous blood supply

MicroCT-based evaluation of vascular network

Blood vessel size distribution of both the ON^+ samples and the control samples was reconstructed in 3-D for presentation based on mapping color-coded scales. The control samples showed normal vascular network, whereas the ON^+ samples showed a blocked stem vessel surrounded by small disconnected vessels and disseminated leakage substance (Microfil) (Fig. 6A). Quantitatively, histograms were compiled to show the blood vessel size frequency distribution in both ON^+ samples and the controls. As compared to the control samples, the necrotic ones showed an increase in small, collateral-sized vessels (200–400 μm) (based on vessel size relative to that of the control

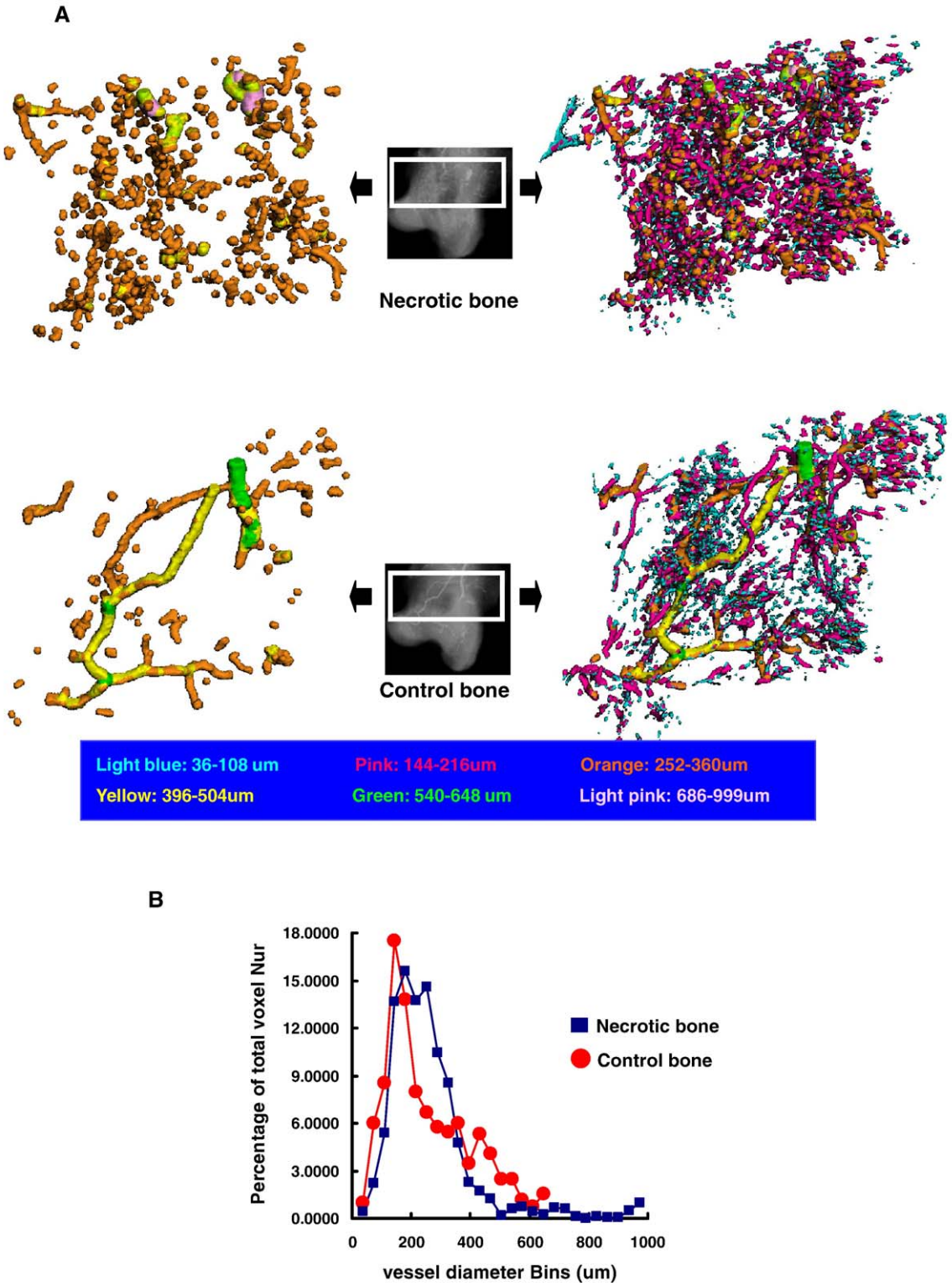

Fig. 6. (A) Representative images of microCT reconstructed 3-D microangiography of proximal femur from a necrotic (upper) and control rabbit (down), which were evaluated from the region of interest (ROI) within the white frame, respectively (refer to Fig. 2 for the definition of ROI). As compared with control specimen, the necrotic one demonstrated blocked stem vessels with numerous disconnected small vessels and disseminated formless radiopaque substances by leaking in downriver region. Note: the left two images were generated from its corresponding left ones after removing the disconnected small blood vessels by removing the vessels with diameter smaller than 252 μm for better visualization of the blocked stem vessels in necrotic specimen. (B) Representative histogram with distribution of blood vessel sizes in both control and necrotic sample. Relative to the control sample, the necrotic sample has more small, collateral-sized vessels (200–400 μm) (based on vessel size relative to that of the control specimen), reduced perfusion to conduit vessels (400–600 μm) and dilated vessels (800–1000 μm).

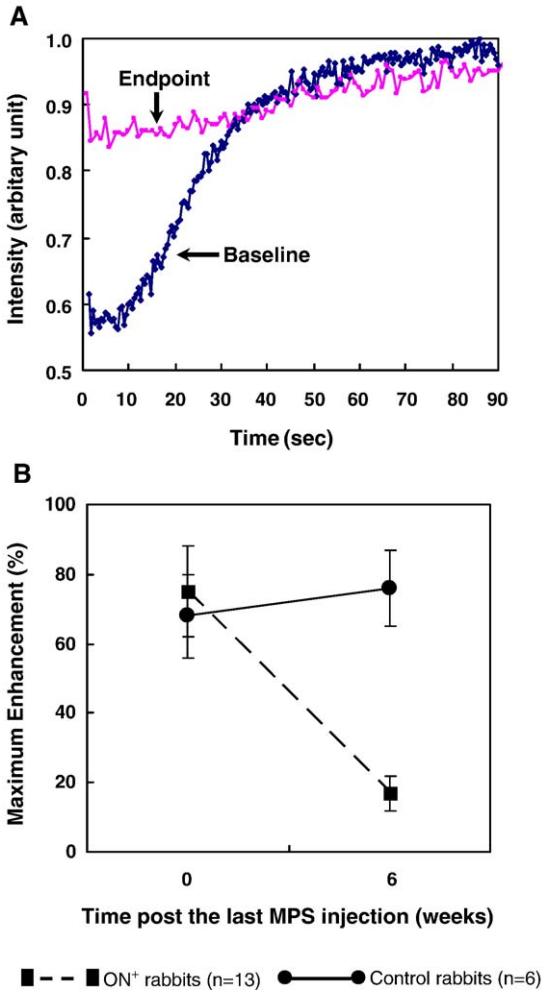

Fig. 7. (A) Representative dynamic MRI time–intensity curves of a rabbit with osteonecrotic proximal femur. Significant decrease in the perfusion index 'maximum contrast enhancement' found at the end of the experiment as compared with its baseline. (B) Time-course changes in perfusion index 'maximum contrast enhancement' of proximal femur analyzed using the repeated ANOVA. Similar to B, significantly decreased perfusion index 'maximum contrast enhancement' found at proximal femur of the necrotic rabbits as compared with that of controls. *$P<0.05$, compared with baseline and control rabbits, respectively (data in mean and SD).

specimen), reduced perfusion to conduit vessels (400–600 μm) and dilated vessels (800–1000 μm) (Fig. 6B).

Dynamic MRI-based perfusion function

A significant decrease ($P<0.05$) in the 'Maximum enhancement' of both proximal and distal femur was found in the ON^+ rabbits as compared with baseline, whereas no significant change ($P>0.05$) was found in the control rabbits (Figs. 7A–B). A moderate decrease in the perfusion index 'maximum enhancement' at both sides was found in the ON^- rabbit as compared with baseline.

Discussion

The present study employed both conventional and advanced static and dynamic bioimaging methods to investigate the effect of the purposed inductive protocol on pathogenic events, pathophysiologic pathways and end-point measures of ON in terms of its incidence and animal mortality.

Intravascular events in pathogenesis of steroid-induced ON

In the present study, the time-course changes in ON^+ rabbits showed a significant decrease in both APTT and ratio of t-PA/PAI-I 24 h after LPS injection as compared with the baseline. Twenty four hours after the last MPS injection, the decreasing tendency for APTT maintained, whereas a rapid decreasing tendency in ratio of t-PA/PAI-I presented. This suggested that LPS induced both hypercoagulable and hypofibrinolytic state. In vitro study of others supported the mechanism that LPS was able to induce hypercoagulable and/or hypofibrinolytic state partially through reduction of endothelia expression of thrombomodulin (TM) [19]. In fact, endothelial TM was an important intermediary substance, which directly or indirectly participated in both inhibition of coagulation and promotion of fibrinolysis, while APTT indicated coagulation function and the ratio of t-PA/PAI-I reflected balance between anti-fibrinolysis and pro-fibrinolysis [20].

Our study also showed that hypofibrinolysis was enhanced by subsequent MPS injections, which in turn resulted in intravascular thrombosis as evidenced histopathologically. The formation or presence of intravascular thrombosis was well demonstrated by microCT-based microangiography, where the thrombi blocked the perfusion as visualized by disconnected vasculatures of the necrotic lesions in decalcified 3-D microCT intraosseous vascular network. In a pilot study, the investigators also explored if the clinical angiography using radiopaque substance barium sulfate would be a more appreciated approach to monitor the steroid-associated emboli formed in intraosseous vascular network. However, due to its larger particle size with rather lower solubility in solution, only blood vessels larger than 250 μm were visualized perfused radiographically. Microfil (lead chromate) is a radiopaque solution with a smaller particle size, which was recently used for quantitative microCT analysis of collateral vessel development after ischemic injury [16] and successfully adopted into the present microCT angiographic study. Based on the scan resolution selected, intraosseous vessels in both proximal and distal femur larger than 36 μm were demonstrated and quantified for comparison. As the microCT available for this study is an in vitro model and the lead chromate is a toxic substance not for in vivo application, we employed dynamic MRI into the current study to monitor the local perfusion disturbance of corresponding skeletal sides.

Extravascular marrow events in pathogenesis of steroid-induced ON

Abnormal lipid metabolism is frequently observed in animals treated with LPS [10,21], although the exact mechanism remains unclear. In the present study, the time-course changes in plasma ratio of LDL/HDL in ON^+ rabbits showed a significantly increased ratio from the baseline 24 h later after

LPS injection; and the tendency was further significantly enhanced 24 h later after the last MPS injection. A higher LDL/HDL ratio was regarded reflecting the prominent lipid transport to the peripheral tissues [22–25]. This might imply that there was a synergetic effect of LPS and MPS on lipid transport to bone marrow. The lipid transport resulting form the higher LDL/HDL ratio might have induced intraosseous hyperlipidemic state, which eventually lead to extravascular marrow compression from lipid deposit. This was evidenced in our histopathological findings, which demonstrated increased fat cell size in the necrotic marrow and accompanied with substantially reduced marrow space for maintaining important functional marrow elements.

Interestingly, the present study also demonstrated more disconnected small vessels associated with angiogenesis and vasculogenesis and more disseminated formless radiopaque substance leaked into the downriver regions of the necrotic bone. This might imply that the neo-vasculature formed in the repair process in this rabbit model was both structurally and functionally abnormal. It has been the consensus that any tissue growth or repair relies on functional mature vasculature. The abnormal neo-vasculature found in this study might be used as a measure to investigate potential intervention strategies developed for treatment of steroid-associated ON by evaluating its role in facilitating the restoration of vascular network from the abnormal neo-vasculature in repair of ON lesion. Collectively, both intravascular and extravascular events contributed to the impaired perfusion function of intraosseous blood supply system, as this was evidenced by the significantly decreased 'maximum enhancement', an index of local blood perfusion measured by dynamic MRI in ON^{+} rabbits in the present study. Similar findings were also reported in an early MRI study on ischemic femoral head in pig model [26].

Confirmation of the proposed effective steroid-associated ON inductive protocol with higher incidence but no mortality

The end-point evaluations in the present study demonstrated that the proposed treatment protocol induced a high incidence of ON of 93%, which was two-fold higher than that of 43% reported by others using a single injection of high-dose MPS (H-MPS × 1) [8]. Also as demonstrated, our inductive protocol resulted in no animal death (zero mortality) as compared with an up to 50% mortality reported using a protocol of two injections of high-dose LPS combined with subsequent three injections of high-dose MPS (H-LPS × 2 + H-MPS × 3) [9]. According to the etiology of steroid-associated ON, the lower ON incidence by the protocol (H-MPS × 1) was due to lack of LPS-induced pre-thrombosis state before steroid treatment [18]. On the other hand, the higher mortality by the protocol (H-LPS × 2 + H-MPS × 3) was due to high-dose-LPS-induced severe endotoxin shock [9]. Since a single low-dose injection of LPS could induce a high incidence of ON with low mortality [10], the present study developed a protocol by modifying the reported protocol (H-LPS × 2 + H-MPS × 3) by replacing the two high-dose LPS injection with a single low-dose LPS injection. The high incidence and even no mortality using this protocol might attribute to both combined administration of LPS–MPS and a single low-dose LPS. The significance of the protocol with high ON incidence but low or no mortality was obvious, at least including both reduction of number of experimental animals required for intervention studies and increase in validity of the evaluation results.

A model for testing medications developed for prevention of steroid-induced ON

To date, no subchondral bone collapse has been demonstrated in ON experimental models irrespective of animal species, steroid dosage and exposure duration and local structural and mechanical condition (bipeds vs. tetrapeds) [8,9,27]. However, this does not imply that ON animal models, such as the current rabbit model, are not suitable for studying pathogenesis, testing the efficacy of agents and intervention strategies developed for prevention of steroid-associated ON. In the present study, we demonstrated many histopathological and pathogenetic features of steroid-induced ON in rabbits similar to those observed in human ON prior to subchondral bone collapse [28]. Histopathologically, ON lesions were presented in multi-focal regions, including locations at both proximal and distal femur. In addition, reparative appositional bone formation also presented around the necrotic bone and reparative fibrous granulation tissues were found next to the necrotic bone resorption. Pathogenically, both intravascular thrombosis and extravascular marrow lipid deposit were found in the model. These evidences strongly supported that the steroid-induced rabbit ON model as the one developed using a unique inductive protocol would be effective to test efficacy of medications developed for prevention of steroid-associated ON for clinical application and confirmation of their long-term effects in prevention of subchondral bone collapse at hip. In fact, this is similar to OVX rat model, which has become a gold standard for preclinical efficacy studies of medications developed for prevention and treatment of osteoporosis, although without being able to result in spontaneous fractures frequently occurred in osteoporotic patients [29].

Conclusion

The present experimental study showed that our experimental protocol with a single injection of low-dose LPS and subsequent pulsed high-dose MPS injections was an effective one to induce ON in rabbits with high incidence and even no mortality. The static and dynamic biomaging modalities, including both conventional histomorphometry and advanced dynamic MRI and microCT-based angiography, were a unique and advanced combination to reveal the pathogenesis–pathophysiology of steroid-associated ON.

Acknowledgments

This study was supported by a Direct Research Grant of the Chinese University of Hong Kong (Project ID Ref. 6901559) and RGC (CUHK4503/06M).

References

[1] So LK, Lau AC, Yam LY, Cheung TM, Poon E, Yung RW, et al. Development of a standard treatment protocol for severe acute respiratory syndrome. Lancet 2003;361:1615–7.

[2] Scribner AN, Troia-Cancio PV, Cox BA, Marcantonio D, Hamid F, Keiser P, et al. Osteonecrosis in HIV: a case–control study. J Acquir Immune Defic Syndr 2000;25:19–25.

[3] Griffith JF, Antonio GE, Kumta SM, Hui DS, Wong JK, Joynt GM, et al. Osteonecrosis of hip and knee in patients with severe acute respiratory syndrome treated with steroids. Radiology 2005;235:168–75.

[4] Penzak SR, Formentini E, Alfaro RM, Long M, Natarajan V, Kovacs J. Prednisolone pharmacokinetics in the presence and absence of ritonavir after oral prednisone administration to healthy volunteer. J Acquir Immune Defic Syndr 2005;40:573–80.

[5] Assouline-Dayan Y, Chang C, Greenspan A, Shoenfeld Y, Gershwin ME. Pathogenesis and natural history of osteonecrosis. Semin Arthritis Rheum 2002;32:94–124.

[6] Lieberman JR, Berry DJ, Montv MA, Aaron RK, Callaghan JJ, Rayadhyaksha A, et al. Osteonecrosis of the hip: management in the twenty-first century. J Bone Joint Surg Am 2002;84:834–53.

[7] Saito S, Saito M, Nishina T, Ohzono K, Ono K. Long-term results of total hip arthroplasty for osteonecrosis of the femoral head. A comparison with osteoarthritis. Clin Orthop Relat Res 1989;244:198–207.

[8] Yamamoto T, Irisa T, Sugioka Y, Sueishi K. Effects of pulse methylprednisolone on bone and marrow tissues: corticosteroid-induced osteonecrosis in rabbits. Arthritis Rheum 1997;40:2055–64.

[9] Yamamoto T, Hirano K, Tsutsui H, Sugioka Y, Sueishi K. Corticosteroid enhances the experimental induction of osteonecrosis in rabbits with Shwartzman reaction. Clin Orthop Relat Res 1995;316:235–43.

[10] Irisa T, Yamamoto T, Miyanishi K, Yamashita A, Iwamoto Y, Sugioka Y, et al. Osteonecrosis induced by a single administration of low-dose lipopolysaccharide in rabbits. Bone 2001;28:641–9.

[11] Ficat RP. Idiopathic bone necrosis of the femoral head. Early diagnosis and treatment. J Bone Joint Surg Am Br 1985;67:3–9.

[12] Kawai T, Sakurabayashi I, Koide A, Kubota N. Fractional quantitation of serum beta-lipoprotein by a simple turbidimetric method. Protides of the biological fluids. Oxford: Pergamon Press; 1978. p. 415–8.

[13] Sugiuchi H, Uji Y, Okabe H, Irie T, Uekama K, Kayahara N, et al. Direct measurement of high-density lipoprotein cholesterol in serum with polyethylene glycol-modified enzymes and sulfated alpha-cyclodextrin. Clin Chem 1995;41:717–23.

[14] Chen WT, Shih TT, Chen RC, Lo HY, Chou CT, Lee JM, et al. Blood perfusion of vertebral lesions evaluated with gadolinium-enhanced dynamic MRI: in comparison with compression fracture and metastasis. J Magn Reson Imaging 2002;15:308–14.

[15] Qin L, Mak ATF, Cheng CW, Hung LK, Chan KM. Histomorphological study on pattern of fluid movement in cortical bone in goats. Anat Rec 1999;255:380–7.

[16] Duvall CL, Robert Taylor W, Weiss D, Guldberg RE. Quantitative microcomputed tomography analysis of collateral vessel development after ischemic injury. Am J Physiol Heart Circ Physiol 2004;287: 302–10.

[17] Prophet EB, Mills B, Arrington JB, Sobin LH, editors. Armed forces institute of pathology laboratory methods in histotechnology. Washington, D.C.: American Registry of Pathology; 1992. p. 98.

[18] Briguet A, Courdier-Fruh I, Foster M, Meier T, Magyar JP. Histological parameters for the quantitative assessment of muscular dystrophy in the MDX-mouse. Neuromuscul Disord 2004;14:675–82.

[19] Glueck CJ, Freiberg RA, Wang P. Role of thrombosis in osteonecrosis. Curr Hematol Rep 2003;2:417–22.

[20] Moore KL, Andreoli SP, Esmon NL, Esmon CT, Bang NU. Endotoxin enhances tissue factor and suppresses thrombomodulin expression of human vascular endothelium in vitro. J Clin Invest 1987;79:124–30.

[21] Dahlback B, Villoutreix BO. The anticoagulant protein C pathway. FEBS Lett 2005;579:310–6.

[22] Fong YM, Marano MA, Moldawer LL, Wei H, Calvano SE, Kenney JS, et al. The acute splanchnic and peripheral tissue metabolic response to endotoxin in humans. J Clin Invest 1990;85:1896–904.

[23] Matsui M, Saito S, Ohzono K, Sugano N, Saito M, Takaoka K, et al. Experimental steroid-induced osteonecrosis in adult rabbits with hypersensitivity vasculitis. Clin Orthop Relat Res 1992;277:61–72.

[24] Michelsen K. Pressure relationships in the bone marrow vascular bed. Acta Physiol Scand 1967;71:16–29.

[25] Motomura G, Yamamoto T, Miyanishi K, Jingushi S, Iwamoto Y. Combined effects of an anticoagulant and a lipid-lowering agent on the prevention of steroid-induced osteonecrosis in rabbits. Arthritis Rheum 2004;50:3387–91.

[26] Lang P, Jergesen JE, Genant HK, Moseley ME, Schuylte-Monting J. Magnetic resonance imaging of the ischemic femoral head in pigs. Dependency of signal intensities and relaxation times on elapsed time. Clin Orthop Relat Res 1989;244:272–80.

[27] Wang GJ, Cui Q, Balian G. The Nicolas Andry award. The pathogenesis and prevention of steroid-induced osteonecrosis. Clin Orthop Relat Res 2000;370:295–310.

[28] Plenk Jr H, Gstettner M, Grossschmidt K, Breitenseher M, Urban M, Hofmann S. Magnetic resonance imaging and histology of repair in femoral head osteonecrosis. Clin Orthop Relat Res 2001;386:42–53.

[29] FDA. Guidelines for Preclinical and Clinical Evaluation of Agents Used in the Prevention or Treatment of Postmenopausal Osteoporosis. Division of Metabolism and Endocrine Drug Products, Food and Drug Administration (FDA), USA, 1997.